Strength Characteristics Of Lightweight Reinforced Concrete Deep Beams With Web Openings

Eman Abdallah H. Abdelaal[1)], Hamed Shaker H. Askar[2)] and Mohamed E. El-zoghiby[3)]
[1] Teaching Assistant, [2] Prof. of Concrete Structures, [3]Associate Prof. of Concrete Structures,
Structural Engineering Department, Mansoura University, El-Mansoura, Egypt.

ABSTRACT

The present experimental investigation reports test results of six lightweight reinforced concrete deep beams with web openings including a reference solid beam. The used concrete in casting the specimens has a cylinder compressive strength of 32MPa. The beams were tested to failure under two-point loads that lie at beams shear span to determine their shear strengths. The main parameter considered in this investigation was the size of web openings. Obtained test results showed a reduction in the beam shear strength relative to the increasing in the opening size. Based on the experimental and obtained results, concluding remarks were drawn. Owing to the obtained results, an experimental equation had been adopted and showed an accepted agreement with the authors specimens and the results of specimens available in literature. Additionally, and owing to the observed crack patterns of tested beams, strut-and-tie models were generated and used to verify the experimental results.

Keywords: Deep Beams; Lightweight Concrete; Shear Strength; Openings; Strut-and-Tie Modeling.

1. INTRODUCTION

There are many structural advantages to use lightweight concrete (LWC) as a building material. The reduction of dead weight due to a lower density of concrete can improve the seismic resistance capacity of building structures (Bogas 2013); (Gao 2015); and (Gesoğlu 2004). Furthermore, the smaller and lighter elements of precast concrete are preferred because the handling and transporting system becomes less expensive. Offshore structures which mostly used for oil production, require LWC elements to provide easier towing and greater buoyancy (Kayali 2008). As a result, there has been growing interest in the practical application of LWC for structural members (Yang 2011), (Wu 2014), and (Wu 2018). In addition (Yang 2006), (Lu 2013), and (yang 2011) also proposed different shear models for deep beams.

Openings are frequently placed in the web region of reinforced concrete (RC) deep beams to facilitate essential services such as access, conduits, AC lines, etc. These openings may interrupt the load path and can cause a sharp decrease of serviceability and strength of RC deep beams (Yang 2007).

Though the strength evaluation and reinforcement details around openings are essential considerations, their design details have not been yet provided by most codes of practice particularly for LWC; (ACI 318-14), (CSA 2014), (CEB-FIP 2010), and (CIRIA 1977).

Experimental tests showed that diagonal cracks can develop just above and below openings. This is due to high stress concentration at opening corners. High transverse tensile strain at diagonal crack zone, would accelerate the decreasing rate of the effective strength of concrete (Tan 2004).

Based on the experimental results of tested specimens, an empirical equation has been adopted and applied to the results of the tested specimens and the results available in literatures. Comparison between the experimental results and the calculated results showed an expected agreement. In addition, the conservatism of strut-and-tie models (STMs) recommended by code provisions such as (ACI 318-14), (CSA 2014), (ECP 2017), and (EC2 2004), and those proposed by (Tan and Cheng 2006) is examined against the variation of openings size.

2. RESEARCH SIGNIFICANCE

Obviously, openings are provided to deep beams to enable essential services and accessibilities to pass. This paper helps to understand the effect of opening size on the LWC beam's shear strength when openings interrupt the load path. A strut-and-tie modeling approach was, also, used to recompute the shear strength of the tested beams.

3. EXPERIMENTAL PROGRAM

3.1 Details of tested specimens

An experimental program was carried-out on specimens with details shown in Table 1. The main parameter of study in this investigation was the opening size. The geometrical details of tested specimens are indicated in Fig. 1.

The beams have an overall depth, h, of 600mm, a span length, L, of 1000mm, and a web thickness, b, of 160mm. Three specimens with web openings having the same depth, m2h, of 180mm, while the other beams with web openings having the same width, m1a, of 200mm.

3.2 Study parameter

The opening size was selected to be the parameter of study to evaluate its effect on the shear strength of the considered deep beams. Table 1 shows the geometrical properties and concrete compressive strength of the tested beams. The beams were subdivided into two main groups according to the opening depth and width, 0.3h and 0.66a, respectively.

3.3 Details of reinforcement

The arrangement of steel reinforcement of the tested beams is as shown in Fig. 2. The main bottom reinforcement was continuous over the beam length. It consists of four bars of 16mm diameter and welded to 160×100×10mm two end plates to provide anchorages. Top reinforcement, in contrast, was two bars of 6mm diameter.

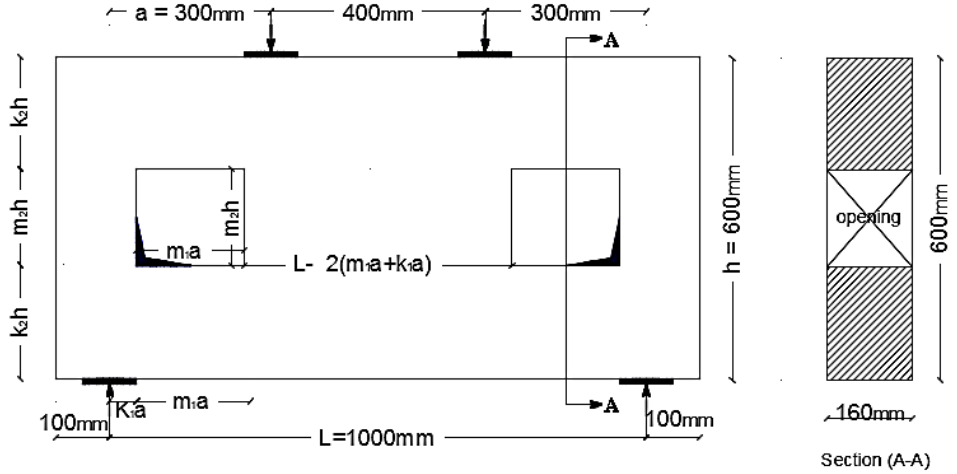

Fig. 1 Typical specimen geometry and dimensions.

Table 1 Details of the tested specimens.

Specimen designation	f_c', MPa	Dimensions, mm			a/h	Opening size, mm				Opening position, mm	
		L	a	h		m_1	m_2	m_1a	m_2h	k_1a	k_2h
B0	32	1000	300	600	0.50	----	----	----	----	----	----
B1						0.33	0.30	100	180	100	210
B2						0.50	0.30	150	180	75	210
B3						0.66	0.30	200	180	50	210
B4						0.66	0.35	200	210	50	195
B5						0.66	0.40	200	240	50	180

Horizontal and vertical web reinforcement are bars of 6mm diameter and spaced at 120mm. Inclined reinforcing bars are laid in two rows above and below openings, each having three bars of 10mm. The V- and diagonal-shaped inclined reinforcing bars are arranged at an angle of 45 degrees to the horizontal axis of beams and placed symmetrically just above and below openings.

4. PROPERTIES OF USED MATERIAL

For quality control purposes, all specimens were tested after 28-days and a cylinder compressive strength f_c' of 32MPa for lightweight concrete was obtained. The concrete mix proportions are shown in Table 2. The structural lightweight concrete having an oven-dry density of 1980kg/m3.

The mechanical properties of the used reinforcing steel are shown in Table 3, where NMS, HGS, f_y, f_u, and E_s are normal mild steal, high grade steal, yield strength, ultimate tensile strength, and elastic modulus of reinforcing steel, respectively.

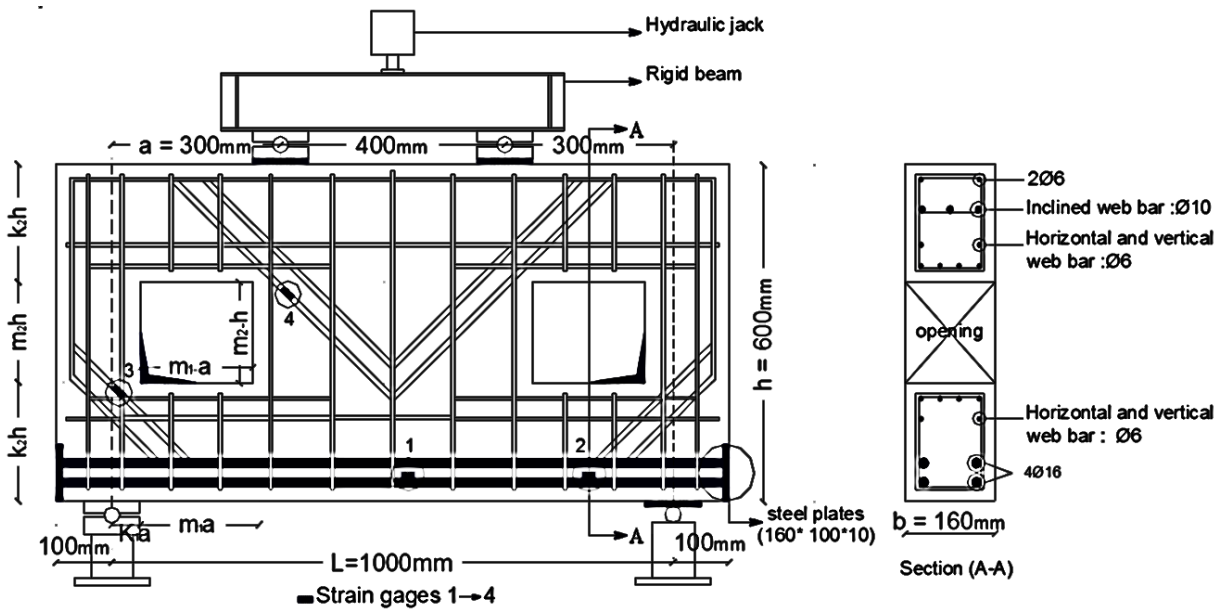

Fig. 2 Typical steel reinforcements arrangement and details.

Table 2 Concrete mix design (cylinder compressive strength f_c'= 32MPa).

	Mixture proportion	Dry weight, kN/m3
Standard type-10 portland cement	1.00	4.9
Silica fume	0.18	0.9
Water	0.33	1.62
Sand	1.048	5.14
Coarse aggregate	0.59	2.9
Light coarse aggregate (lika)	0.918	4.5
Super plasticizer (sikament165)	0.046	0.23
Glass fiber	0.018	0.09
Traseal DM	0.01	0.05

Table 3 Mechanical properties of Reinforcing steel.

Steel type	f_y, MPa	f_u, MPa	E_s, MPa
NMS	240	350	200000
HGS	400	600	200000

5. TEST SET-UP AND INSTRUMENTATION

The specimens were tested using a large closed steel frame. All were connected together by two large channels. A hydraulic jack having a 2000kN capacity was used in applying load to tested specimens. Four strain gauges having 10mm length were used for each specimen to measure the strain at critical sections of reinforcing steel bars, as shown in Fig . 2.

6. TESTING PRODUCER

The All beams were tested to failure under a two-point top loading system with a loading intervals of 20kN/minute. Each tested beam was supported on a hinged support at the left and a roller support at the right. At the load and support points of application, a steel plate with 20mm thickness was provided to prevent bearing failure of the loaded beam.

The description of both the test set-up and the considered loading system are shown in Fig. 3. Vertical deflections δ (at specimen mid-span) were measured using linear variable differential transducers (LVDT) mounted at the bottom face of the tested beams.

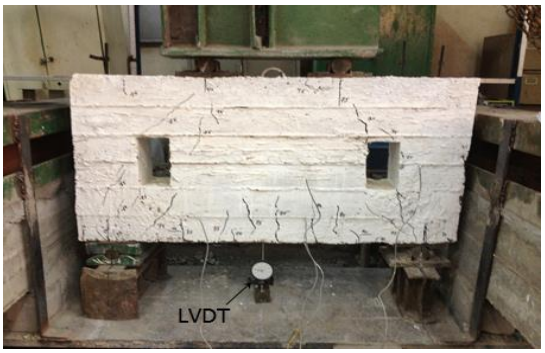

Fig. 3 Test set up and loading system.

7. EXPERIMENTAL RESULTS AND DISCUSSIONS

7.1 Crack propagation

Figs. 4 , and 5 showed the idealized crack pattern in the tested beams. In which, 1 refers to flexural cracks, 2 to corner cracks, 3 to an arch-rib cracks, and 4 to diagonal cracks, respectively.

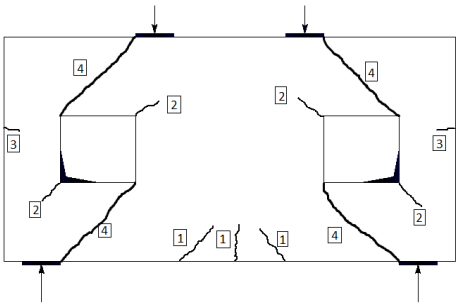

Fig. 4 Idealized cracks in deep beams with web openings.

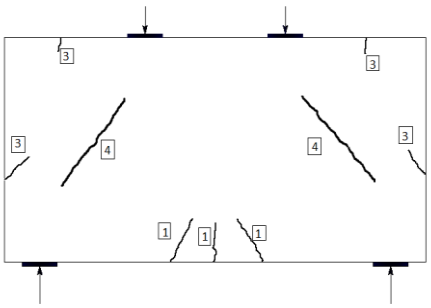

Fig. 5 Idealized crack pattern in solid reference beam.

Fig . 6 Crack patterns and failure modes of tested beams.

The first crack appears in all tested beams at opening corners, propagated towards the applied points of load with increasing in load. Flexural cracks started to appear at the beam mid-span just after initiation of the first crack. After words, the diagonal cracks originated at opposite corners of openings. The arch-rib cracks appeared on all tested beams just before approaching the ultimate load capacity

The diagonal cracks, especially those formed below openings led directly to beams failure, as shown in Fig. 6. The crack patterns which observed above and below the openings were almost identical and illustrate the concrete struts connecting loading points, web openings and support points. This observation is

used to validate the geometry of concrete struts in the proposed strut-and-tie model for the tested beams.

7.2 Effect of web opening on both cracking and ultimate loads

The cracking and ultimate loads for tested beams are recorded in Table 4. Additionally, the corresponding moment at mid-span are also recorded. It could be seen that the beam moment decreased by increasing the opening dimensions. The cracking-to-ultimate load ratio (P_{cr}/p_{ult}), also, decreased as the opening size increased by about 23 to 40%.

The relation between the opening size and the cracking and ultimate loads are shown in Fig. 7. It illustrates that the reduction in stiffness was slightly predominant in beams having openings with the same depth m_2h = 0.3h than those having the same width m_1a = 0.66a. This indicates that the width of opening has a significant influence on the cracking and ultimate loads, while the variation in stiffness has not.

Table 4 Cracking and ultimate loads.

Beam No.	L, mm	P_{cr}, kN	M_{cr}, kN*m	P_{ult}, kN	M_{ult}, kN*m	p_{cr} / p_{ult} (%)	Type of Failure
B0	1000	850	425	1100	550	77	Shear Failure
B1		750	375	1000	500	75	
B2		600	300	850	425	70.5	
B3		400	200	600	300	66.6	
B4		320	160	500	250	64	
B5		180	90	300	150	60	

The ability of a beam to sustain further loading after the formation of the first crack depends on whether these cracks would penetrate into concrete zones at the loading and support points. The test results showed that the ultimate strength depends on the opening size which reduces the strut width joining the bearing plates at the support and loading points.

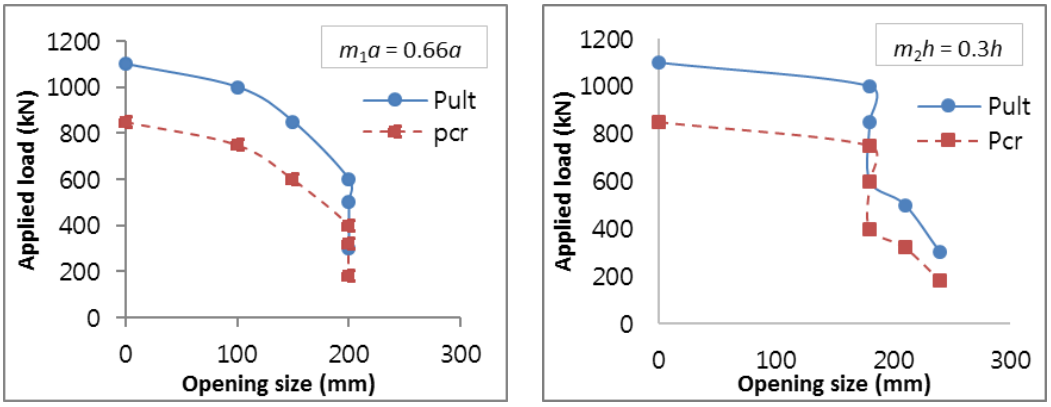

Fig. 7 Effect of web opening size on applied load.

The ultimate strength of deep beams is affected only when the direct force path from the loading to the support points is interrupted with opening. In such a case, two alternative force paths can be identified to carry the applied force to the support, led to shear failure. This means that the ultimate shear strength of the beams with small openings as those of B1, has a light effect compared with the ultimate shear strength of solid beam.

7.3 Deflection and strain observations

7.3.1 Mid-span Deflection

Mid-span deflections of tested beams versus the applied load are shown in Fig. 8. The development of flexural cracks in the region of maximum moment had a minimal influence on the stiffness of the tested beams. The development of diagonal cracks caused an decrease in deflections for beams with openings than that of the reference beam by about 18 to 54%.

The reduction in stiffness after the formation of diagonal cracks was more predominant in beams having opening with the same depth m_2h = 0.3h than those having the same width m_1a = 0.66a by about 38% and 8%, respectively. This indicates that the width of opening size influence significantly in both the beam behavior and stiffness, Figs. 8 and 9.

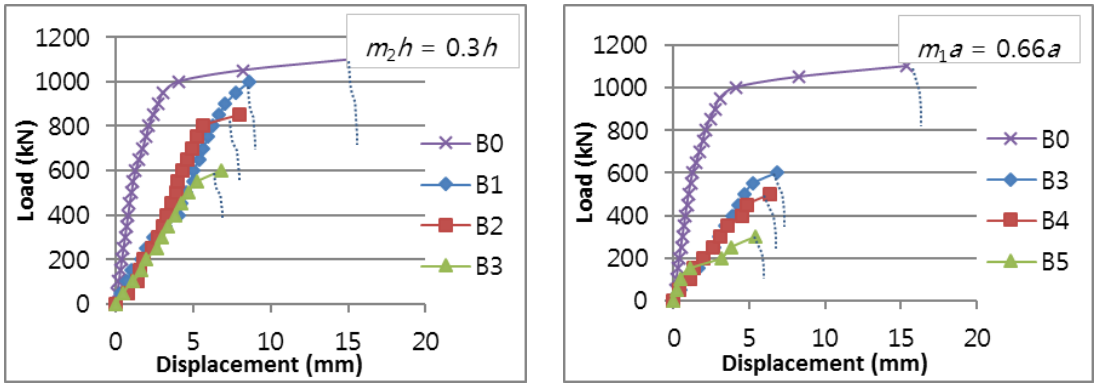

Fig. 8 Load deflection relationship at beam mid-span.

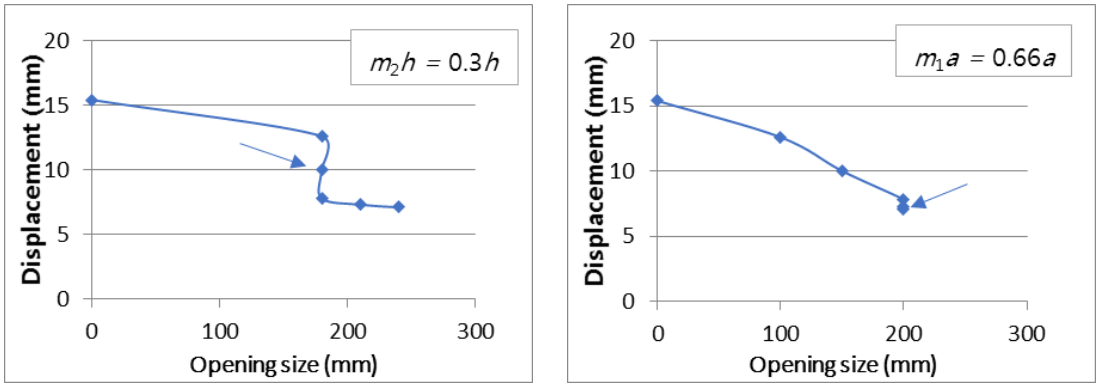

Fig. 9 Web opening size versus mid-span deflection.

7.3.2 Strain energy of tested specimens

The readings of steel strains of four strain gauges embedded inside beams, are shown in Figs. 10 and 11. It showed the strain records at positions 1 and 2 for bottom reinforcement and positions 3 and 4 for inclined reinforcement. It was subdivided into two main groups based on the opening depth and width, $m_2h = 0.3h$ and $m_1a = 0.66a$, respectively.

In Figs. 10 and 11 the strain development of bottom reinforcement at flexural cracks and that of inclined reinforcement at diagonal cracks are plotted versus the applied load. The strains in inclined reinforcement quickly developed with the occurrence of diagonal cracks as expected. This amount of the developed strain was strongly dependent on propagation of these diagonal cracks.

For the shear reinforcement, the strain in bottom reinforcement for position 2 at mid-shear span was higher than that for position 1 at beam mid-span and the strain in the inclined reinforcement for position 3 at bottom of openings was higher than that for position 4 at top of openings.

Strains of all bottom and inclined reinforcing steel reached the yield strain before the expected ultimate shear strength, as shown in Figs. 10 and 11. This indicates that the inclined reinforcements effectively transverse tensile stresses across the diagonal cracks.

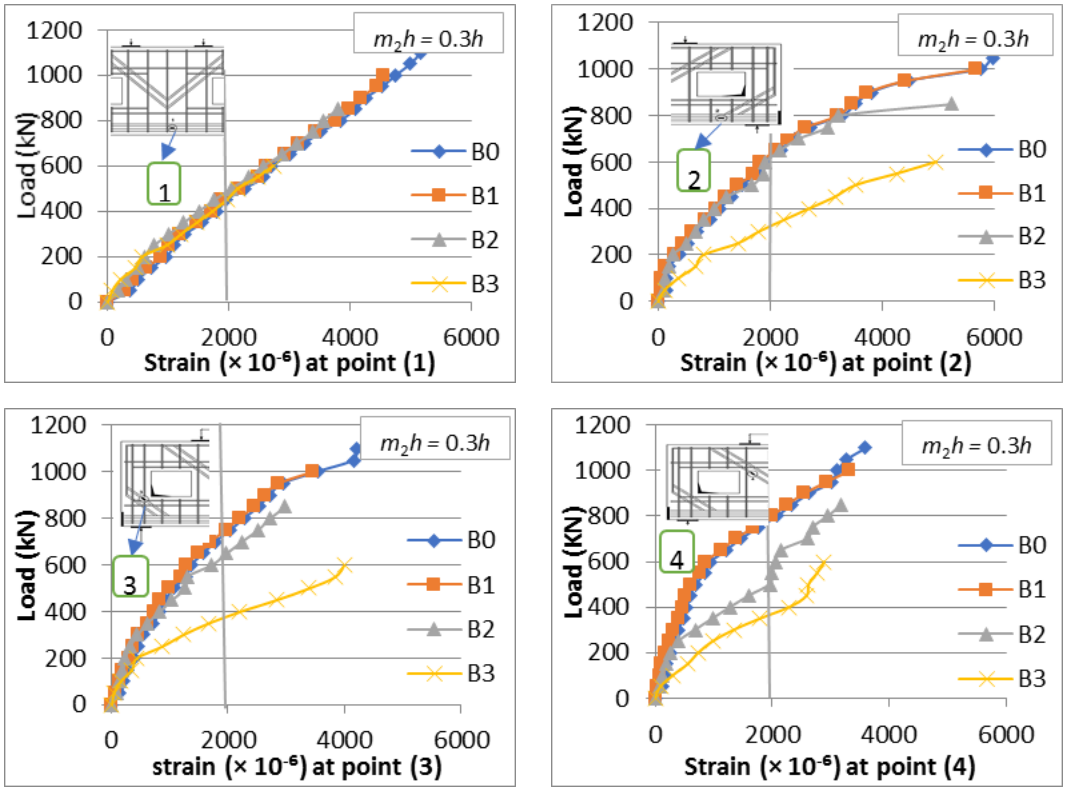

Fig. 10 Strain in reinforcement versus the applied load at points 1 to 4 with $m_2 h = 0.3h$.

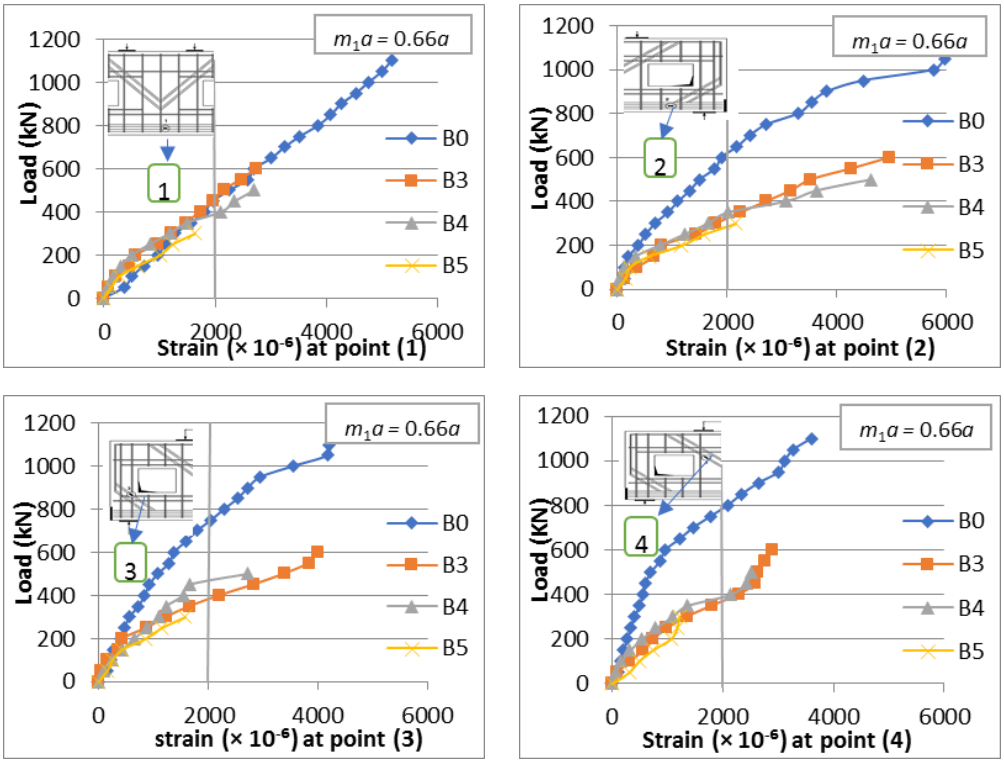

(**B** refers to tested beam designation)

Fig. 11 Strain in reinforcement versus the applied load at points 1 to 4 with $m_1\ a = 0.66a$.

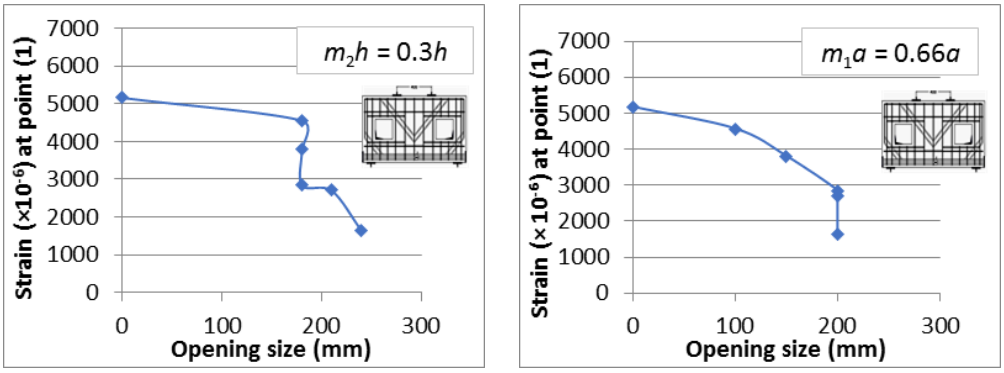

Fig. 12 Web opening size versus strain in bottom reinforcement at point 1.

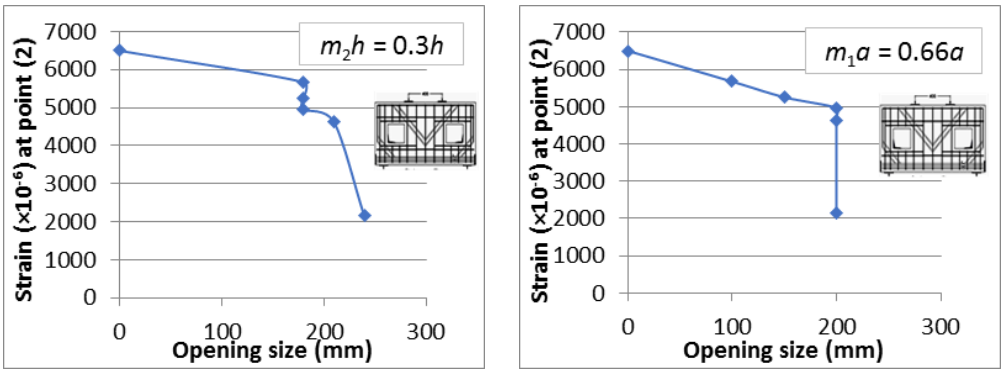

Fig. 13 Web opening size versus strain in bottom reinforcement at point 2.

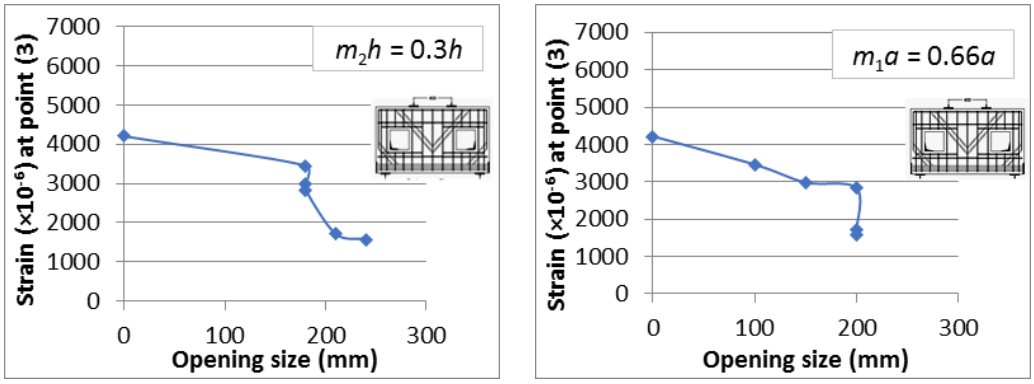

Fig. 14 Web opening size versus strain in inclined reinforcement at point 3.

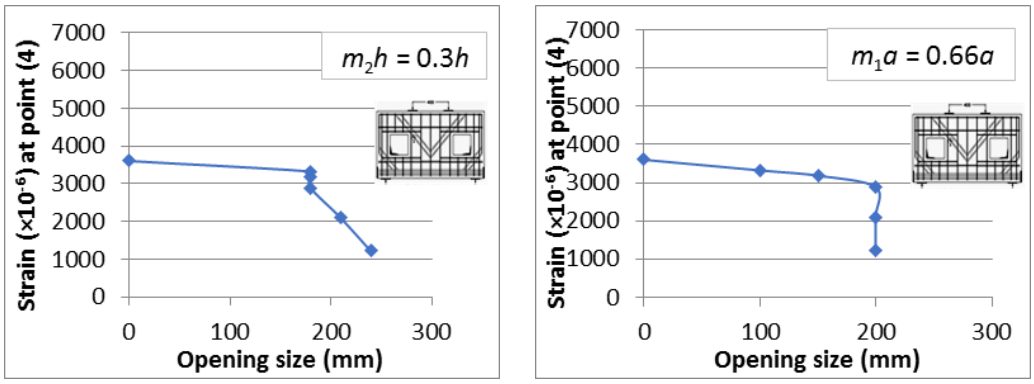

Fig. 15 Web opening size versus strain in inclined reinforcement at point 4.

Figs. 12 to 15 presenting the strain measurements against the opening size. The figures illustrate that the strain in bottom reinforcement decreased by increasing the opening size at points 1 and 2 by about 68.4% and 66.8%, respectively. The strain in the inclined reinforcement decreased by increasing the opening size at points 3 and 4 by about 62.7% and 66.2%, respectively. This indicates that the width of opening size has a significant influence on the strain behavior at different places in bottom and inclined reinforcement.

8. EXPERIMENTAL EQUATION FOR ESTIMATION BEAMS FAILURE LOAD

Based on the experimental results of tested beams and using the regression analysis the relationship between a failure load ratio P_n/P_o and beams specification, the concrete cube compressive strength f_{cu}, opening area, and reinforcement ratios was proposed and illustrated in Fig 16. The ultimate load P_n can be obtained using Eq(2) as follows:

$$\frac{P_n}{P_o} = 1.3 - 0.02 * \left(\frac{\sqrt{f_{cu} * \rho_{oA}}}{\sqrt{2E_s * \rho_s * \rho_s'}}\right) \quad (1)$$

$$P_n = P_o * [1.3 - 0.02 * \left(\frac{\sqrt{f_{cu} * \rho_{oA}}}{\sqrt{2E_s * \rho_s * \rho_s'}}\right)] \quad (2)$$

where E_s is the elastic modulus of reinforcement, $\rho_{oA} = \frac{A_{op}}{b \times h} = m_1 \times m_2$ is the opening area to shear span area ratio, $\rho_s = \frac{A_s}{b \times d}$ and $\rho_s' = \frac{A_s'}{b \times d}$ are the flexural ratio of the main and inclined reinforcements, respectively.

9. COMPARISON OF PROPOSED EQUATION AND EXPERMINTAL FAILURE LOAD

To investigate the applicability of the proposed equation, the predicted and experimental values of the failure load P_n for the tested specimens were compared with the results available in literature (Yang2007). The comparison is shown in Table 5 and Fig. 17. The mean and standard deviation of the predicted-to-experimental failure load $((P_n)_{Eq}/ (P_n)_{Exp})$ obtained. The predictions obtained from the proposed equation shows a good agreement.

Table 5 Details of test results and predictions.

Researches	Spec.	Details of openings			f_{cu},	Reinforcement				Moment M_n, kN.m		$\frac{(M_n)_{eq.}}{(M_n)_{Exp.}}$
		m_1	m_2	ρ_{oa}	Mpa	Inclined	Main	ρ_s'	ρ_s	Exp.	Eq.	
Author specimens	Bo	---	---	---	41	6ϕ10	4ϕ16	0.0055	0.0093	1100	1100	1
	B1	0.33	0.3	0.099		6ϕ10	4ϕ16	0.0055	0.0093	1000	1000.2	1
	B2	0.5	0.3	0.15		6ϕ10	4ϕ16	0.0055	0.0093	850	778.7	0.92
	B3	0.66	0.3	0.198		6ϕ10	4ϕ16	0.0055	0.0093	600	570.3	0.95
	B4	0.66	0.35	0.231		6ϕ10	4ϕ16	0.0055	0.0093	500	427.04	0.85
	B5	0.66	0.4	0.264		6ϕ10	4ϕ16	0.0055	0.0093	300	283.7	0.95
yang and Ashour specimens (2007)	No	---	---	---	68	---	3ϕ19	---	0.0098	1583.3	1583.3	1
	T1-1	0.25	0.1	0.025		3ϕ10	3ϕ19	0.0027	0.0098	1666.7	1673.6	1.004
	T1-2	0.25	0.1	0.025		6ϕ10	3ϕ19	0.0055	0.0098	2361.1	1866.3	0.79
	T3-3	0.25	0.3	0.075		9ϕ10	3ϕ19	0.0082	0.0098	1916.6	1674.1	0.87
	F1-2	0.5	0.1	0.05		6ϕ10	3ϕ19	0.0055	0.0098	1805.5	1674.3	0.93
	F1-3	0.5	0.1	0.05		9ϕ10	3ϕ19	0.0082	0.0098	2222.2	1802.1	0.8
	F3-3	0.5	0.3	0.15		9ϕ10	3ϕ19	0.0082	0.0098	1444.4	1289.8	0.89
											Mean	0.92
											Standard deviation	0.07

Based on the above, it could be observed that the concrete strength, f_{cu}, was the predominant parameter and not the type of concrete. Furthermore, based on the results of tested specimen B2 and reference specimen F3-3 (Yang 2007), it was observed that there is a difference in the behavior of lightweight and normal

concrete in deflection; four-times in lightweight concrete than that in normal concrete.

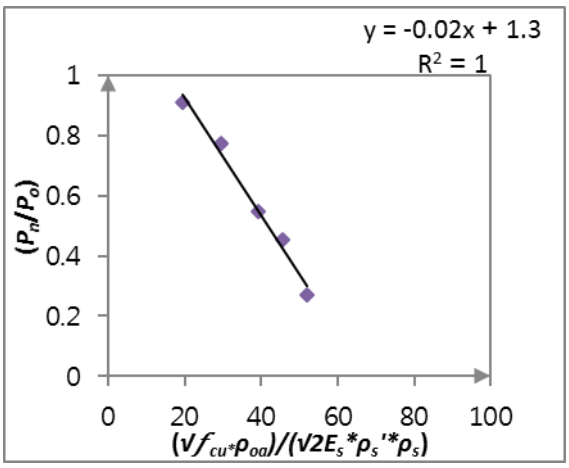

Fig. 16 Failure Load ratio from Eq(2).

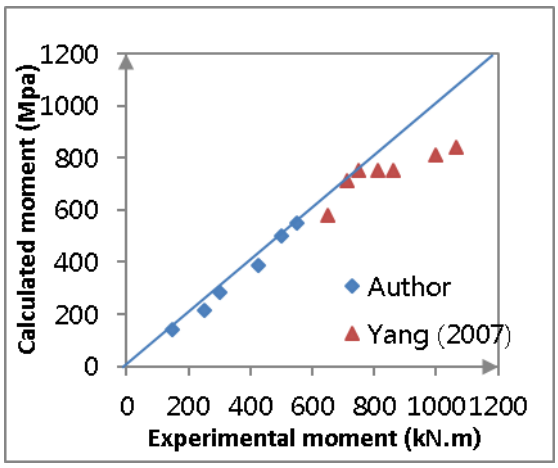

Fig. 17 Relationship between calculated and experimental load.

10. STRUT TIE MODELLING

10.1 Verification Examples

10.1.1 Case study I, STM-I

Numerical scheme for Beam B_0:

The LWC reference deep beam B_0 (without openings) along with two concentrated loads applied at its top are shown in Fig. 18. Input data h = 600mm, d = 540.5mm, b = 160mm, and $b_1 = b_2$ = 100mm. The shear span-to-depth ratio a/h = 300/600 = 0.5 and f_c' = 32MPa (LWC). The main steel is 4Φ16 (A_s = 804.25mm^2), the inclined steel is 3Φ10 (A_{si} = 471.23mm^2), and f_y = 400MPa.

1. <u>The internal lever arm, L_d</u>:

The height a_1 of node N_1 in Fig. 18c is $n\emptyset_{bars} + 2c + (n-1)s$

where n is the number of steel layers, $\emptyset_{bars}$ is diameter of the main steel, c is the clear cover, and s is the clear distance between bars. Thus, $a_1 = 2 \times 16 + 2 \times 25 + (2-1)18 = 100\text{mm}$. The width of strut S_2 (w_2 or a_2, Fig. 18c) when assuming $T_{1n} = T_{1n,\,max}$ where $T_{1n,\,max}$ = max nominal strength of tie T_1 if $f_s = f_y$ is $T_{1n} = A_s f_y = 804.25 \times 400 \times 10^{-3} = 321.69\text{KN}$.

Since $T_{1n} = S_{2n}$ or simply $T_1 = S_2$. Then, $321.69\text{ kN} \times 1000 = 0.85\beta f_c' b a_2 = 0.85 \times 1 \times 32 \times 160 \times a_2$ or $a_2 = 73.92\text{mm}$. Thus, $L_d = h - 0.5\,(a_1 + a_2)$ or 600 - 0.5 (100 + 73.92) = 513.04mm.

1. <u>Angle of inclined strut, α_1</u> :

With reference to Fig. 18b, $\alpha_1 = \tan^{-1}\frac{L_d}{a} = \tan^{-1}\frac{513.04}{300} = 59.68^o$

2. <u>Width of struts:</u>

In Fig. 18, the width of strut S_1 can be calculated as:

- The width w_{11} of strut S_1 at the lower node N_1 is $a_1 \cos\alpha_1 + b_1 \sin\alpha_1$ or $100 \times \cos 59.68 + 100 \times \sin 59.68 = 136.8$mm.
- The width w_{12} of strut S_1 at the upper node N_2 is $w_{12} = a_2 \cos\alpha_1 + b_2 \sin\alpha_1$ or $73.92 \times \cos 59.68 + 100 \times \sin 59.68 = 123.63$mm
- The width of strut S_2 at the upper node N_2 is w_2 or $a_2 = 73.92$mm.

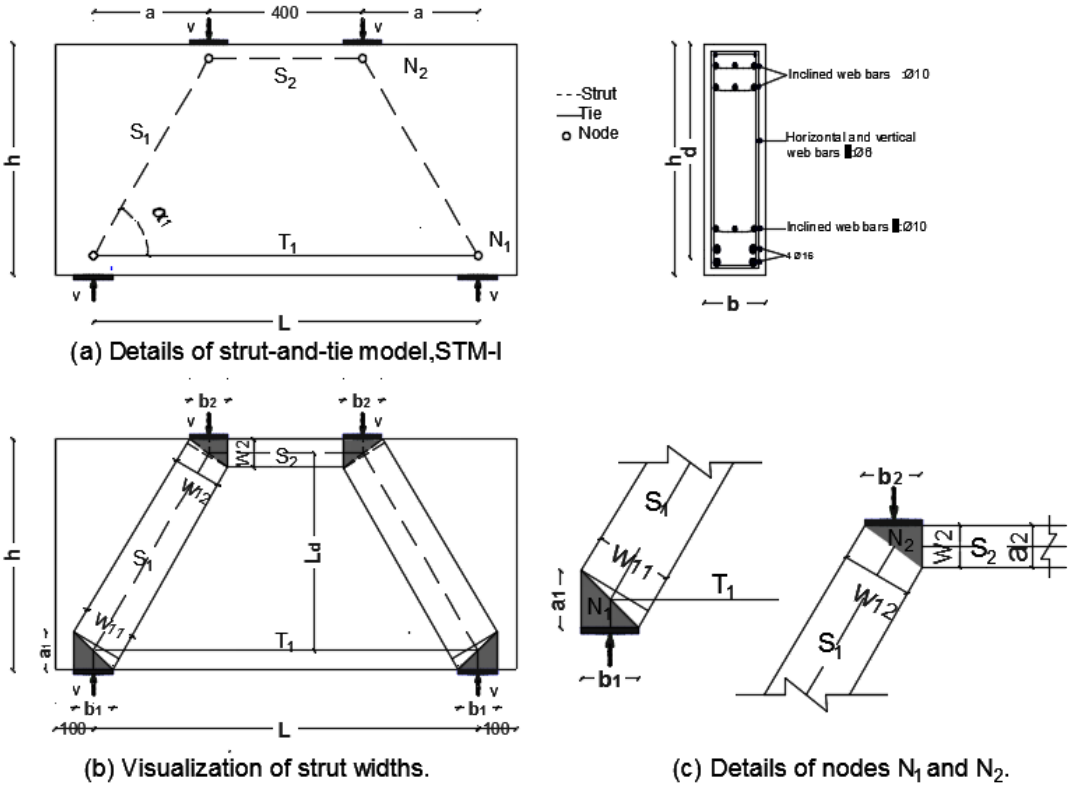

Fig. 18 Solid deep beam B_0.

3. STM forces:

Assuming that the tie T_1 will reach its f_y and from equilibrium we obtain (Table 6): $T_{1n,\,max} = A_s f_y = 804.25 \times 400 \times 10^{-3} = 321.69$ kN. Try $T_{1n} = T_{1n.\,max} = 321.69$kN. From equilibrium, $V_n = T_{1n} \times \frac{ld}{a} = 321.69 \times \frac{513.04}{300} = 550.13$ KN and simply, $S_1 = \frac{T_1}{\cos\alpha 1} = \frac{321.69}{\cos 59.68} = 637.22$kN. Finally, $P_{STM} = 2V_n = 2 \times 550.13 = 1100.26$kN.

Table 6 Calculated member forces for STM-I

Model Label	Force, kN	T or C	Notes
S_1	637.22	C	C = Comp. or Strut T = Tension or Tie
S_2	321.69	C	
T_1	321.69	T	

Checking of stress limits:

a. Concrete struts:

Knowing that f_c' = 32MPa, the effective strength of a strut, $f_{ce}^{s} = 0.85 f_c' \beta_s$ is:

$f_{ce}^{s1} = 0.85 f_c' \beta_{s1} = 0.85 \times 32 \times 0.75 = 20.4$MPa, for Strut S_1

$f_{ce}^{s2} = 0.85 f_c' \beta_{s2} = 0.85 \times 32 \times 1.00 = 27.2$MPa, for Strut S_2

The max nominal strength of the struts is given by, $S_{in.\ max} = f_{ce}^{si} b w_i$, i = 1, 2.

Horizontal strut S_2:

No need to check S_2 as its width (w_2 or a_2) was found based on $S_{2n} = T_{1n,\ max}$.

Inclined strut S_1:

- The maximum nominal strength of strut S_1 or $S_{11n,\ max}$ at the lower node N_1 is:
  $0.85 f_c' (\beta_{s1} \text{or } \beta_{n1}) b w_{11} = 20.40 \times 160 \times 136.8 \times 10^{-3} = 446.51$kN.
- The maximum nominal strength of strut S_1 or $S_{12n,\ max}$ at the upper node $N_2$is:
  $0.85 f_c' (\beta_{s1} \text{or } \beta_{n2}) b w_{12} = 20.40 \times 160 \times 123.63 \times 10^{-3} = 403.52$kN.

$S_{1n,\ max}$ = the smaller value of $S_{11n,\ max}$ and $S_{12n,\ max}$ or 403.52kN. Since S_{1n} or or $637.22 > S_{1n.\ max}$ or 403.52 (unsafe), assume a new adjusted value of $S_{1n}$and repeat from Step 1. Try $S_{1n} = S_{1n,\ max}$ or 403.52kN. Thus, $S_{2n} = T_{1n} = S_{1n} \times \cos\alpha_1 = 403.52 \times \cos\alpha_1 = 403.52 \cos\alpha_1$ kN which will be less than $S_{2n,\ max}$ or 321.69kN which is okay.

1. The internal lever arm, L_d:

Using a trial-and-error, try $T_{1n} = 198\text{kN} = S_{2n} = 0.85 \times 32 \times 1 \times 160 \times a_2$ or $a_2 = 45.5$mm. $L_d = h - 0.5\ (a_1 + a_2)$ or 600 – 0.5 (100 + 45.5) = 527.25mm.

2. Angle of inclined strut, α_1:

$\alpha_1 = tan^{-1} \frac{L_d}{a} = tan^{-1} \frac{527.25}{300} = 60.36^{o}$.

3. Width of struts:

$w_{11} = 100 \times \cos 60.36 + 100 \times \sin 60.36 = 136.36$mm.

$w_{12} = 45.5 \times \cos 60.36 + 100 \times \sin 60.36 = 109.42$mm.

4. STM forces:

Try $T_{1n} = S_{2n} = 198$kN. $S_{1n} = \frac{T_{1n}}{\cos\alpha} = \frac{198}{\cos 60.36} = 400.36$kN which is slightly less than $S_{1n,\ max}$ or 403.52kN, which is okay. Also, $V_n = T_{1n} \times \frac{ld}{a} = 198 \times \frac{527.25}{300} = 347.98$kN which is slightly less than $V_{n,\ max}$ or 348.16kN, which is okay.

b. Nodes:

The maximum node capacity is $f_{ce}^{ni} b w_i$ where $f_{ce}^{ni} = 0.85 f_c' \beta_{ni}$. Table 7 summarizes the calculations performed for the effective concrete nodes. Finally, P_{STM} = 2 V_n = 2× 347.98 = 695.96kN. Since the measured collapse load was $P_{EXP} = 2P$ = 1100kN; then, $\frac{P_{STM}}{P_{EXP}}$ is about 65%.

Table 7 Summary of effective concrete node calculations.

Node Label	Type	β_n	Surrounding forces, kN			Available width, mm	f_{ce}^{ni}, MPa	Max. nominal strength, kN	Satisfaction
N1	CCT	0.8	S_1	400.36	C	136.36	21.76	474.75	yes
			V_n	347.98	C	100		348.16	yes
			T_1	198	T	100		348.16	yes
N2	CCC	1.00	P_n	347.98	C	100	27.2	435.2	yes
			S_1	400.36	C	109.42		476.19	yes
			S_2	198	C	45.5		198	yes

Case study II, STM-II

Numerical scheme for Beam B_1:

The LWC deep beam with openings along with two concentrated loads applied at its top are shown in Fig. 19. Input data h = 600mm, d = 540.5mm, b = 160mm, and b_1 = b_2 = 100mm. The ratio a/h = 300/600 = 0.5, the opening width m_1a = 100mm, opening depth m_2h =180mm, and f_c' = 32MPa. The main steel is 4Φ16 (A_s = 804.25mm^2), the inclined steel is 3Φ10 (A_{si} = 471.23mm^2), and f_y = 400MPa.

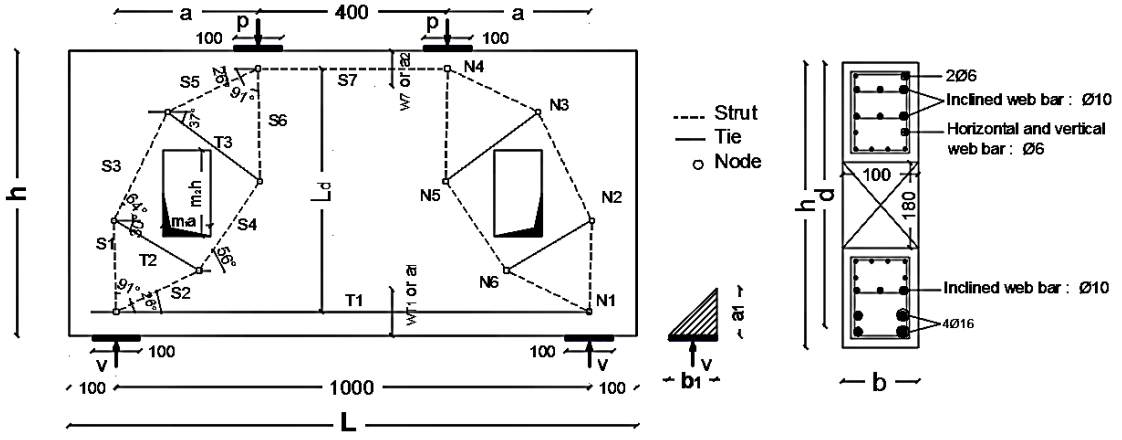

Fig. 19 Proposed STM-II.

1. <u>Geometrical parameters:</u>

The previously showed crack patterns in Fig. 6 can be used when setting-up the strut-and-tie model for the tested beams. In Fig. 19, the width of the tie T_1 (height of node N_1) is:

$w_{T_1} = a_1 = n\emptyset_{bars} + 2c + (n-1)s = 2 \times 16 + 2 \times 25 + (2-1)18 = 100$mm.

The nominal max strength of the tie T_1 or $T_{1n,\,max}$ is $A_s\, f_y = 804.25 \times 400 = 321.7$kN. The widths of the ties T_2 and T_3 (each is 2 × 3Φ10) can be computed from $2 \times 10 + 2 \times 25 + (2-1)18 = 88$mm. The nominal strength of T_2 is $A_s\, f_y = 471.23 \times 400 = 188.49$kN. The width of strut S_7 (w_7 or a_2) can be computed from $T_{1n,\,max} = S_{7n}$. Then, $A_s\, f_y = 0.85 f_c' \beta_s b a_2 = 804.25 \times 400 = 0.85 \times 32 \times 1 \times 160 \times a_2$ or $a_2 = 73.92$mm, L_d = 600 – 0.5 (100 + 73.92) = 513.04mm.

2. Reactions:

From equilibrium: $V_n = T_1 \times \frac{ld}{a} = 321.7 \times \frac{513.04}{300} = 550.13\text{kN}$.

3. Model Geometry and Forces

Trying $T_1 = T_{1n,max}$ or $A_{s_1} f_y = 804.25 \times 400 = 321.7\text{kN}$ and from equilibrium, the forces in all members can then be obtained, Fig. 20.

4. Effective concrete strength of the struts

Knowing f_c' = 32MPa, the effective strength of a strut, $f_{ce}^s = 0.85 f_c' \beta_s$ is $0.85 \times 32 \times 1.0$ or 27.2MPa for prismatic struts and 20.4MPa for bottle-shaped struts.

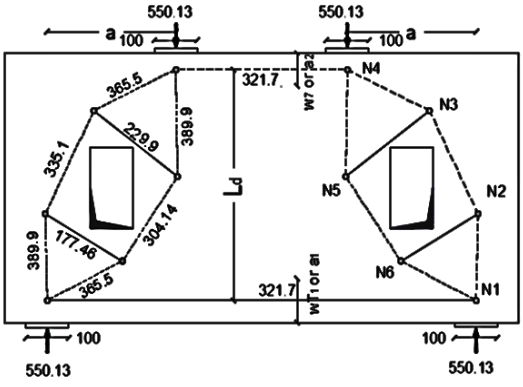

Fig. 20 Computed model forces for STM-II (kN) assuming yielding of T_1.

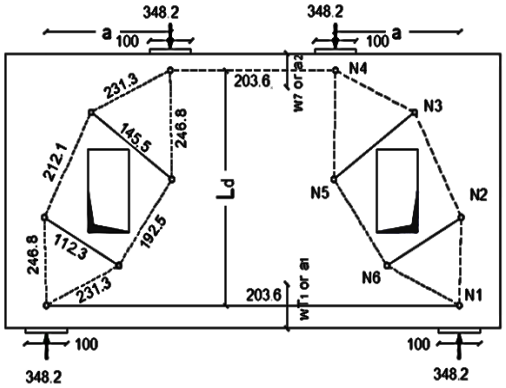

Fig. 21 Computed model forces due to reducing *P* to 348.2kN for STM-II.

5. Effective concrete strength of the nodes

Knowing f_c' = 32MPa, the effective strength of a node, $f_{ce}^n = 0.85 f_c' \beta_n$ is $0.85 \times 32 \times 1.0 = 27.2\text{MPa}$ for *C-C-C* nodes and 21.76MPa for *C-C-T* nodes.

6. Checking the bearing of the nodes

For node 1, the nominal value of the reaction $V_\text{n} = 21.76 \times 160 \times 100 = 348.2\text{kN}$, which is less than 550.13kN, Fig. 20. For node 4, the nominal value of the load $P_\text{n} = 27.2 \times 160 \times 100 = 435.2\text{kN}$, which is less than the force *P* = 550.13kN. Therefore, the load and reaction should be reduced to the smaller value of V_n and P_n or 348.2kNand the force in the tie T_1 is subsequently reduced to 203.6KN and the forces all members are, then, recomputed, Fig. 21.

7. Checking of stresses

***Node* 1:** The bearing stresses has been checked before and, therefore, no need to re-check it again. For struts S_1 and S_2, Fig. 19, the resultant force R_A is 403.31kN and its angle α_A is 59.68° . Thus, its width $w_A = a_1 \cos\alpha_A + b_1 \sin\alpha_A = 100 \times \cos 59.68 + 100 \times \sin 59.68$ or 136.8mm. Then the nominal strength of the strut is $> R_{An} = 20.4^* \times 160 \times 136.8$ or 446.5 kN (*the smaller of the node- and strut-strength), which is R_A or 403.31kN which is okay.

***Node*s 2 and 5:** Because they are very wide and the reinforcement bars have sufficient anchorage lengths, nodes 2 and 5 need not to be checked.

***Node*s 3 and 6:** These two nodes (as they are smeared and the reinforcement bars have sufficient anchorage lengths) need not, also, to be checked.

***Node* 4:** The bearing stresses has been checked before and, therefore, no need to re-check it again. For struts S_5 and S_6, the resultant force R_B = 403.31kN and its angleα_B is 59.68°. Thus $w_B = a_2 \cos\alpha_A + b_2 \sin\alpha_A = 73.92 \times \cos 59.68 + 100 \times \sin 59.68$ or 123.64mm . Then, the max nominal strength of the struts is > $R_{An} = 27.2 \times 160 \times 123.64 = 538.08$kN, which is R_B or 403.31kN. Finally, P_{STM} = 2 V_n = 2 × 348.2 = 696.4kN. Since the measured collapse load was $P_{EXP} = 2P =$ 1000kN ; then, $\frac{P_{STM}}{P_{EXP}}$ is about 70%. Additionally, the equation load $P_{Eq} =$ 909.2kN; then , $\frac{P_{STM}}{P_{Eq}}$ is about 77%, this indicates that the experimental and the proposed equation results were higher than those with STM .

9. CONCLUSIONS

In the present experimental investigation, six lightweight RC deep beams with web openings (including a reference solid beam) were tested to failure. All tested beams have two web openings located at the center of the shear span which interrupt the concrete strut connecting load and support points. Whereas, when the same opening is located far from the compressive force path, it would have little influence on the beam shear behavior. A strut-tie modeling approach was, also, presented to re-compute the shear strength of the tested beams. The following conclusions may be drawn:

- For all tested beams, the observed crack patterns just above and below the openings were almost identical.
- The variation of opening size affects significantly the propagation of cracks with increasing the applied load.
- The width of opening has a significant influence on the cracking and ultimate loads, and the beam behavior and stiffness.
- The cracking-to-ultimate load ratio decreased with the increase of the opening size by about 23 to 40%.
- The diagonal cracks were decreased in solid deep beams than that having openings. Those formed below the openings can directly leads to beams failure
- The mid-span deflection of LWC deep beams decreased in those with web openings than that of the reference solid beam by about 18 to 54%.
- Strain in steel reinforcement quickly developed with the occurrence of diagonal cracks and decreased by increasing the opening size.
- For the shear reinforcement, the strain in the bottom reinforcement at mid-shear span was higher than that at beam mid-span. The strain in the inclined reinforcement at the bottom of openings was higher than that at the top of openings.
- Based on the obtained experimental results, an experimental equation, to calculate the ultimate shear capacity of tested beams with opening has been proposed.
- The comparison between the experimental results and those obtained from the proposed equation showed an acceptable agreement.

- The behavior of the lightweight concrete in deflection differs from that for normal concrete.
- The strut-and-tie method was used to model the tested deep beams. The shear strengths of the tested beams were higher than those calculated using the strut-tie modeling approach.

REFERENCES

ACI Committee 318, "Building Code Requirements for Structural Concrete (ACI318-14) and Commentary (318R-14)," American Concrete Institute, Farmington Hills, MI, USA.

Bogas J. A. and Gomes A. (2013), "Compressive behavior and failure modes of structural lightweight aggregate concrete characterization and strength prediction," *Mater. Des*., Vol. 46, 832–841.

CEB-FIP, (2010), "Design of Concrete Structures," CEB-FIP Model Code 2010, Thomas Telford, London, UK.

CSA Building Code (2014), "Design of Concrete Structures," Structures (Design)- A National Standard Association, Toronto, Ontario, Canada.

CIRIA, (1977), "The Design of Deep Beams in Reinforced Concrete Structures (CIRIA 2)," Ove Arup and Partners and CIRIA, London, UK.

Egyptian Code(2017), "The Design and Construction of Concrete Structure, (ECP 203-2017), Ministry of Housing, Utilities and Urban Communities, National Housing and Building Research Center, Cairo.

Eurocode 2, (2004), "Design of Concrete Structures," EN 1992-1-1:2004, British Standards Institution, London, UK.

Gao Y and Zou C (2015), "Experimental study on segregation resistance of nanoSiO2 fly ash lightweight aggregate concrete," *Constr. Build. Mater.*, Vol. 93, 64–69.

Gesoglu M., Ozturan T. and Guneyisi E. (2004), "Shrinkage cracking of lightweight concrete made with cold-bonded fly ash aggregates," *Cem. Conc. Res.*, Vol. 34(7), 1121–1130.

Kayali, O. (2008), "Fly Ash Lightweight Aggregates in High Performance Concrete," *Constr. Build. Mater.* Vol. 22(12), 2393-2399.

Lu, WY, Lin, J. and Yu, HW. (2013), "Shear strength of reinforced concrete deep beams," *ACI Str. J*., Vol. 110(4), 671–680.

Tan, K. H., Tang, C. Y., and Tong, K. (2004), "Shear Strength Predication of Pierced Deep Beams with Inclined Web Reinforcement," *Mag. Conc. Res*., V. 56, No. 8, 443-452.

Tan, K. H., and Cheng, G. H., (2006) "Size Effect on Shear Strength of Deep Beams: Investigating with Strut-and-Tie Models," Journal of Structural Engineering, ASCE, V. 132(5), 673-685.

Wu, T., Lv, BB. and Liu, X. (2014), "Test On High-Strength Lightweight Aggregates Concrete Deep Beams With Shear Span-To-Depth Ration Variations," 13th Inter. Symposium on *Str. Eng.*, Vol1 and II, 12-19.

Wu, T., Wei, H. and Liu, X. (2018), "Experimental Investigation Of Shear Models For Lightweight Aggregate Concrete Deep Beams," *Str. Eng.*, Vol. 21(1), 109-124.

Yang, K. H., Chung, H. S., Eun, H. C., and Ashour, A. F., (2006) "Influence of Web Openings on the Structural Behavior of Reinforced High-Strength Concrete Deep Beams," *Str. Eng.*, Vol. 28, 1825-1834.

Yang, K. H., Heon-Soo Chung, H. S., and Ashour, A.F (2007), "Influence of Inclined Web Reinforcement on Reinforced Concrete Deep Beams with Openings," *ACI Str. J.*, Vol. 104(5)580-589.

NOTATION

L	Length of deep beam
d	Depth of deep beam
b	Width of deep beam
a	Shear span
h	Overall depth of deep beam
m_1, m_2	Coefficients of opening size
K_1, K_2	Coefficients of opening position
m_1a	Width of opening
m_2h	Depth of opening
L_p	Width of loading plate
B	Number of tested beam designation
f_c'	Cylinder compressive strength of concrete
f_{cu}	cube compressive strength of concrete
f_y	Yield strength of reinforcing steel
f_u	ultimate strength of steel bar
E_s	Elastic modulus of reinforcing steel
NMS	Normal mild steel
HGS	High Grade steel
δ	Displacement at beams mid-span
p_{cr}	Critical load
p_{ult}	Ultimate load
M_{cr}	Moment at critical load
M_{ult}	Moment at ultimate load
ρ_{oa}	Area ratio of the opening to shear span
ρ_s	Flexural ratio of the main reinforcement
ρ_s'	Flexural ratio of the inclined reinforcement
A_s	Area of the main reinforcement
A_s'	Area of the inclined reinforcement
V_n	Shear strength